ASSESSMENT OF POST-MANEUVER OBSERVATION CORRELATION USING SHORT-ARC TRACKLETS

J. A. Siminski[(1)], T. Flohrer[(1)], and T. Schildknecht[(2)]

[(1)]*Space Debris Office, ESA/ESOC, Darmstadt, Germany, Email: {jan.siminski, tim.flohrer}@esa.int*
[(2)]*Astronomical Institute, University of Bern, Switzerland, Email: thomas.schildknecht@aiub.unibe.ch*

ABSTRACT

Satellites maintain or establish their operational orbit by performing impulsive or continuous thrust maneuvers. When cataloging resident space objects, these rapid or slow orbital changes complicate a successful correlation. The new orbit remains uncertain and cannot be used for operations such as conjunction detection. This work outlines and assesses a method for the correlation of optical tracklets to already cataloged objects and the following orbit recovery. For that purpose, historic orbital data is analyzed to predict possible states after the maneuver using kernel density estimation. The resulting probability density function also provides a measure for the association likelihood of a new tracklet. The methods are tested with optical observations from the Zimmerwald observatory. Maneuver information and ephemerides are reported by the satellite operator and used as a reference.

Keywords: *space situational awareness, correlation, cataloging, maneuvers, short-arc problem, optical observations*.

1. INTRODUCTION

When maintaining a catalog of resident space objects, new measurements must be associated to already cataloged objects. If no matching entry in the catalog is found, the new observations either originate from an unknown object or from a maneuvered spacecraft.

Objects in high-altitude orbits are typically observed with ground-based optical telescopes. Due to limited observation time, each object can only be observed for a short duration. The resulting short observation arcs, called tracklets, do not provide enough information to determine the full orbital state after the maneuver (cf. [10]). The updated orbital state is essential for operational tasks, such as collision avoidance, but is also required in order to find the object again and keep the number of duplicate database entries low. As proposed in [13], a likely candidate state after the maneuver can be obtained by analyzing and characterizing historic data from the object in the catalog to predict the state after the maneuver. The maneuver history can be obtained from satellite operators or estimated from past cataloged states. An example of the latter estimation is given by Lemmens and Krag [5] who detect maneuvers from the publicly available Two-line element catalog (*space-track.org*). Figure 1 shows the time-series of the inclination of Meteosat-9 determined from tracklets. The satellite is observed from the Zimmerwald observatory in Switzerland and serves as a test case throughout this paper. The *North-South* station-keeping maneuver epochs can be approximately computed from the figure by identifying the local peaks. Figure 2 shows the time-series for selected mean orbital elements (using the mean element formulation by Kamel [4]). The elements are derived from the weekly reported reference orbits by EUMETSAT. In addition to the North-South station-keeping as in Figure 1, it also shows other types of maneuvers. In total, the satellite performed one relocation maneuver, seven North-South station-keeping maneuvers, some small *slew* maneuvers, and otherwise *East-West* maneuvers in this time period. The maneuver epochs and types were reported by EUMETSAT by email [9].

Before starting the orbit recovery, the measurements must be first associated to the cataloged objects. Otherwise the catalog size would artificially increase without actually adding any new objects to the domain. For that purpose, the historic data from the figures is used to de-

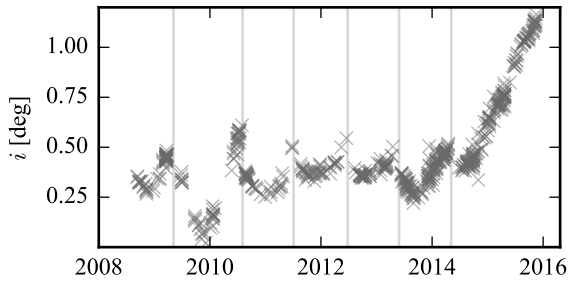

Figure 1: Time series of inclination (i) determined from optical observations of Meteosat-9. Gray vertical lines indicate reported North-South station-keeping maneuvers.

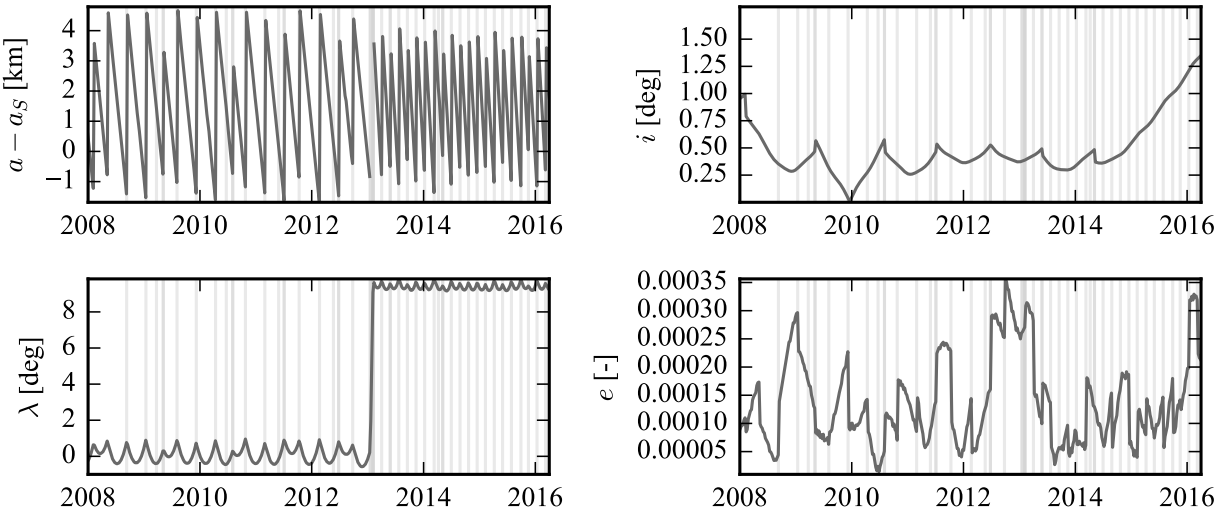

Figure 2: Time series of mean orbital elements for Meteosat-9: semi-major axis a w.r.t. to the synchronous a_S, inclination i, longitude λ, eccentricity e.

scribe the post-maneuver state probability. The resulting density function is then used to compute an association likelihood. Alternatively, Holzinger et al. [2] and Singh et al. [7] propose to use a control effort distance metric to rank different possible object associations, i.e. the object which realizes the measurement with the least fuel consumption is the most likely originator.

After the successful association step, the most likely post-maneuver state is estimated. In [2] the orbital solution which requires the least amount of fuel is considered as a good estimate. However, realizing the new measurement with minimum fuel does not need to return the same optimal result as when performing long-term orbit maintenance maneuver optimization. The approach developed in [13] overcomes this limitation by augmenting the information of the new observation with the probability density function derived from the historic data. The observation correlation and recovery of the most likely orbital state is briefly illustrated with a simulated example. The two possible approaches, i.e. control effort minimization as in [2, 7] and using historic data as in [13], are assessed with reference ephemerides and maneuvers of Meteosat-9 and optical observations from the Zimmerwald observatory collected from 2008 to 2016. The focus of this paper (complementary to the analysis in [13]), is the assessment of the accuracy of the recovered states using the real observations.

2. MANEUVER CHARACTERIZATION

As proposed in [13], maneuvers are characterized with so-called *feature vectors*. The information from the past states before and after the maneuver is compressed in this vector. The vector elements are selected in a way that allows grouping, i.e. values that should be similar for the same type of maneuver.

The feature vector is assembled from the variables described in the following:

1. A maneuver type is dependent on the current orbital elements, e.g. whenever a geostationary satellite reaches its box boundaries in longitude, it will most likely perform an East-West maneuver. Similarly, it will perform a North-South correction when reaching a certain inclination.

2. The change in orbital elements itself also describes the maneuver, e.g. a similar semi-major axis change is typically used for East-West station-keeping.

3. Maneuvers are likely to be performed after similar time-intervals Δt^i (due to similar dynamics causing a deviation from the nominal orbit and due to human operator practice).

4. Station-keeping maneuvers typically repeatedly require the same amount of fuel described with ΔV. For instance, East-West maneuvers, when performed regularly, need a certain ΔV depending on the sub-satellite longitude [14]. Inclination control requires a different amount of fuel and depends on the epoch (due to luni-solar perturbations).

The above explained characteristic variables apply to maneuver strategies with instantaneous changes (which is observable for most of the satellites in the geostationary domain). Continuous thrust orbit control strategies require different variables to group the maneuver types, e.g. the rate of change of orbital elements over time. However, the available dataset contains only satellites with

instantaneous orbital changes. Therefore, this analysis focuses on these maneuver strategies.

For each past maneuver epoch $i = 1 \dots n$, where n is the number of past maneuvers, the feature vector is then given by

$$\boldsymbol{c}^i = (\boldsymbol{e}_b^i, \boldsymbol{e}_a^i, \Delta\boldsymbol{e}^i, \Delta t^i)\,, \tag{1}$$

where $\boldsymbol{e}_b^i$ are the pre-maneuver mean elements (consisting of semi-major axis a, mean longitude λ, inclination i, and eccentricity e), $\boldsymbol{e}_a^i$ are the elements after the maneuver, $\Delta\boldsymbol{e}^i$ is the difference between them and Δt^i is time difference w.r.t. to the last maneuver. Instead of using the full set of orbital elements, a subset is used which is sufficient to describe geostationary orbits.

Figure 3 shows selected components of the feature vectors $\boldsymbol{c}^i$ for all maneuver epochs (illustrated with the $\times$). As also observable in the inclination time series, the points can be grouped into two types of maneuvers: one group has no inclination change (accumulation of many samples in the middle of the bottom plot) and one dispersed group with inclination corrections. A semi-major axis change is likely once a longitude value around $9.5° - 9.7°$ or around $0°$ is reached (upper plot). The latter described group represents the strategy before the relocation in the beginning of 2013. The upper plot also shows that the maneuvers after the relocation are typically performed once every 60 days.

In addition to the samples, the figure also shows an empirical density function based on the points of the sample in the feature vector space. The probability of and the relationship between the characteristic variables is described with the so-called *kernel density estimation* (cf. [11]).

Given any new state after the maneuver $\boldsymbol{e}_a^{n+1}$ at t^{n+1}(described with orbital elements), the probability density can be expressed in terms of the historic feature vectors $\boldsymbol{c}^i$ with the following equation

$$f(\boldsymbol{e}_a^{n+1}) = \sum_i^n w_i\, \boldsymbol{k}_h\, (\tilde{\boldsymbol{c}}^{n+1} - \boldsymbol{c}^i)\,, \tag{2}$$

where $\boldsymbol{k}_h$ is a smoothing kernel function with bandwidth h, w_i are weighting factors, and the tested feature vector

$$\tilde{\boldsymbol{c}}^{n+1} = (\boldsymbol{e}_b^{n+1}, \boldsymbol{e}_a^{n+1}, \Delta\boldsymbol{e}^{n+1}, \Delta t^{n+1})\,. \tag{3}$$

is obtained by combining the latest orbital state in the database $\boldsymbol{e}_b^{n+1}$ with the new state $\boldsymbol{e}_a^{n+1}$ and computing the time difference Δt^{n+1} to the last observed maneuver. Various choices for smoothing kernels $\boldsymbol{k}_h$ are discussed in the literature along with strategies how to select the bandwidth h [12]. Here, a Gaussian kernel is selected with Silverman's rule of thumb for the bandwidth selection. In order to allow for strategy changes (e.g. the relocation), weights are used to decrease the impact of old samples on the density function. A *forgetting factor* ϕ is introduced to scale the kernel. The respective weights are computed with

$$w^i = \phi^{t^{n+1} - t^i}\,. \tag{4}$$

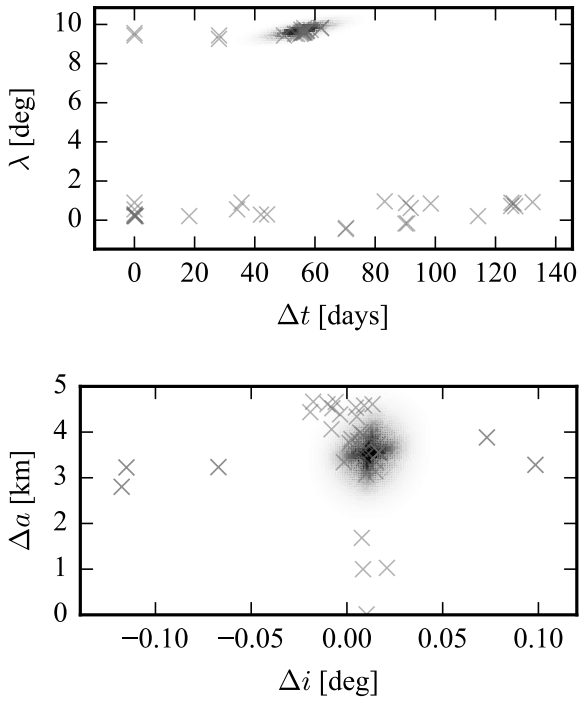

Figure 3: Probability density of orbital changes, pre and post-maneuver states and time since the last maneuver.

The size of the weights thus depends on how old the maneuver of the sample is. A typical choice for ϕ is 0.99. A smaller value will decrease the weight for older samples. This weighting scheme explains why some accumulations in Figure 3 do not contribute much to the empirical density function (e.g. the samples with a longitude λ around $0°$).

3. ASSOCIATION OF NEW OBSERVATIONS AND RECOVERY

After receiving a new tracklet, it must be first associated to a catalogue object. If no match in the catalog is found, the closest objects flagged as a maneuverable spacecraft is assessed. In addition, the probability that they maneuvered or not can be estimated and considered (e.g. as suggested in [6]). The probability that the observation originates from a specific object is then calculated to select the most-likely candidate. If multiple candidate objects can be associated with a similar probability, each one can be loosely associated using the probability as an association weight.

The computation of the likelihood is explained in the following. The cataloged object state before the maneuver is now denoted with $\boldsymbol{e}_b$ at t_b for notational simplicity (dropping the superscript index). A new tracklet at t_a is represented with the line-of-sight $\boldsymbol{s}$ and its time-derivative $\dot{\boldsymbol{s}}$. When augmenting these observation vectors with the

range and range-rate $\boldsymbol{x} = (\rho, \dot{\rho})^\mathsf{T}$, a state hypothesis expressed in orbital elements at t_a is given

$$\tilde{\boldsymbol{e}}_a(\boldsymbol{x}) = \boldsymbol{e}(\boldsymbol{r}, \dot{\boldsymbol{r}})\,, \tag{5}$$

where the position and velocity in the inertial frame are

$$\boldsymbol{r}(\boldsymbol{x}) = \boldsymbol{R} + \rho\boldsymbol{s} \quad \text{and} \quad \dot{\boldsymbol{r}}(\boldsymbol{x}) = \dot{\boldsymbol{R}} + \dot{\rho}\boldsymbol{s} + \rho\dot{\boldsymbol{s}} \tag{6}$$

and $\boldsymbol{R}$ and $\dot{\boldsymbol{R}}$ denote the station position and velocity.

The density function for the post-maneuver state is then computed from inserting Equation (5) into (2)

$$f(\boldsymbol{x}) = \sum_i^n \boldsymbol{k}_h(\tilde{\boldsymbol{c}}(\boldsymbol{x}) - \boldsymbol{c}^i)\,. \tag{7}$$

The approximate Δt is computed from t_a and the last estimated maneuver epoch. All other orbital elements required for $\tilde{\boldsymbol{c}}$ are computed from $\boldsymbol{x}$ and the new observation vectors $\boldsymbol{s}$ and $\dot{\boldsymbol{s}}$. This effectively reduces the high-dimensional feature vector density function to a 2-dimensional one.

The most-likely orbital solution using this density function is then given by

$$\hat{\boldsymbol{x}}_k = \arg\max_{\boldsymbol{x}\in\mathcal{C}} f(\boldsymbol{x}) \tag{8}$$

and consequently if multiple catalog states are tested with one new measurement, the one with the largest probability is the most promising candidate for the association. As the density function in Equation (2) is not necessarily unimodal, the corresponding density function in range and range-rate can be multi-modal as well and thus allows for multiple feasible solutions.

Figure 4 shows the density for a simulated observation of Meteosat-9. A series of observations is simulated using the reference states at the post-maneuver epochs and deriving the line-of-sight and its time-derivative thereof. The reference ephemerides before and after the last maneuver (East-West) of the dataset obtained from the weekly reference orbits. The maximum of the probability density function w.r.t. to the reference solution in the center is indicated with the white cross ($\times$). The error in range and range-rate for this simulated example is around 100 m and 0.1 m/s. The density as shown in Figure 3 is computed from about 50 pre- and post-maneuver states of Meteosat-9 before the last maneuver.

An alternative approach is proposed by Holzinger et al. [2] and Singh et al. [7], where the orbit of a satellite after a maneuver is recovered assuming that the measurement is realized using the least amount of fuel ΔV. Similar to the first approach, a function is optimized to find the most likely candidate. The function and minimum is shown in Figure 5 and is explained in the following paragraphs.

Let $\boldsymbol{e}_b$ at t_b be the known orbital state of a cataloged object right before the maneuver and $\boldsymbol{e}_a$ at t_a the unknown

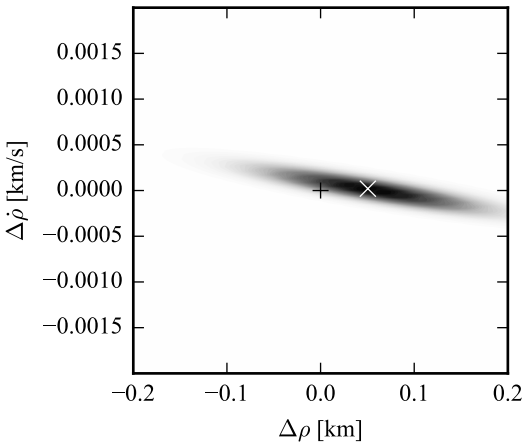

Figure 4: Probability density function of orbital state given a new measurement. Range and range-rate are centered around the reference solution (+). The white cross ($\times$) depicts the maximum of the density function.

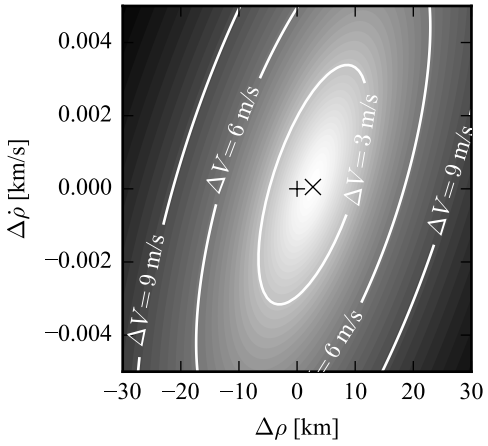

Figure 5: ΔV requirement depending on $\boldsymbol{x}$ (relative to the reference solution (+) in the center). The minimum ΔV solution is depicted with the $\times$.

after it. The fuel consumption is approximated using the quadratic loss [2]

$$P = \min\left\{\frac{1}{2}\int_{t_b}^{t_a} \boldsymbol{u}(t)^\mathsf{T}\boldsymbol{u}(t)\,\mathrm{d}t\right\} \tag{9}$$

where $\boldsymbol{u}$ is the thrust control and is included as an additional acceleration in the equations of satellite motion. The quadratic loss describes the minimum energy solution of a trajectory connecting $\boldsymbol{e}_b$ and $\boldsymbol{e}_a$. It is found with optimal control problem solvers (here the one by Houska et al. [3] is used) and is commonly easier to find than the direct solution giving the smallest possible ΔV. More details about the approach can be obtained from [2, 7, 13].

The required ΔV is bounded with

$$\Delta V(\boldsymbol{e}_b, \boldsymbol{e}_a) \leq \sqrt{2(t_a - t_b)P} \tag{10}$$

and the most likely state after the maneuver, using Equation 5 and the minimum energy trajectory, is accordingly given by

$$\hat{\boldsymbol{x}}_m = \arg\min_{\boldsymbol{x}} \Delta V(\boldsymbol{e}_b, \tilde{\boldsymbol{e}}_a(\boldsymbol{x}))\,. \tag{11}$$

The observed error of the optimal point $\hat{\boldsymbol{x}}_m$ for the simulated example in Figure 5 is approximately one order of magnitude worse when compared to the solution of the first method using historic data.

4. ACCURACY ASSESSMENT

This section compares the accuracy of the resulting post-maneuver state of the kernel-density estimate $\hat{\boldsymbol{x}}_k$ and the ΔV minimum $\hat{\boldsymbol{x}}_m$. The accuracy using simulated observations is discussed in [13]. Here, tracklets collected at the Zimmerwald observatory are used. A set of measurements observed at most 7 days after a maneuver is selected. As occasionally Meteosat-9 is not observed for a longer duration, not every maneuver can be tested in this analysis (compared to when using simulated observations as in [13]). However, the accuracy of the results should be more representative of what is achievable with the methods.

The last 8 maneuver epochs, which fulfill the criterion above, are used to select the states before and after the maneuvers from the weekly orbits. The analysis is performed for the latest maneuvers in the data set in order to guarantee that the empirical density function is sufficiently sampled. The kernel density estimation for each test considers only states in the past. Seven of the observed maneuvers within this sequence are East-West station keeping (EWSK) maneuvers and one is a small slew maneuver (SLEW). The maneuvers and the corresponding tracklet epochs are summarized in Table 1.

The density function and the ΔV-function are optimized using the same numerical optimization routine (*optimize.minimize*) from the SciPy library [8]. The synchronous semi-major axis ($\sim 42,164$ km) serves to compute an initial starter for the optimization. In case of the kernel density function f, a bad starter can fall into a region with numerically zero probability. Hence, the iterative optimizer will not find a gradient or better value in the close vicinity of the starter and will fail to converge. This behavior was only observed when artificially placing starters far away from the solution. However, the density function can be initially sampled on a grid to find the local maxima. From thereon the iterative solvers are capable of finding the most likely solution.

Table 1: Maneuver epochs and observation epochs.

#	*Type*	*Maneuver*	*Observation*
1	EWSK	2014-01-08 07:13	2014-01-08 21:50
2	EWSK	2014-03-11 08:43	2014-03-12 03:49
3	SLEW	2014-04-08 10:58	2014-04-10 03:13
4	EWSK	2014-08-27 05:48	2014-09-01 20:45
5	EWSK	2014-10-22 07:13	2014-10-23 17:55
6	EWSK	2014-12-17 22:58	2014-12-18 23:09
7	EWSK	2015-02-09 06:58	2015-02-10 02:11
8	EWSK	2015-09-29 05:28	2015-09-30 18:47

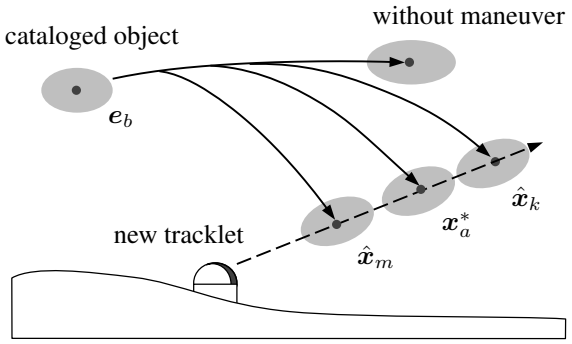

Figure 6: Accuracy assessment using reference range and range-rate $\boldsymbol{x}_a^*$ after maneuver. The different solutions $\hat{\boldsymbol{x}}_m$ and $\hat{\boldsymbol{x}}_k$ are compared to the reference in range - range-rate space.

The difference between reference and obtained solutions is shown with the errors in range and range-rate all selected epochs. The different correlation methods and solutions $\hat{\boldsymbol{x}}_k$, $\hat{\boldsymbol{x}}_m$, and the reference $\boldsymbol{x}^*$, are illustrated in Figure 6. All points lie on the same line-of-sight and have the same topocentric angular velocity. The comparison results are shown in Figure 7.

The kernel density function estimate predicts the reference state after the maneuver better by one order of magnitude. This relative performance difference agrees with the theoretical assessment in [13] using only simulated observations. Due to errors in the tracklets, the overall accuracy decreased when compared to the previous analysis.

5. CONCLUSIONS

The accuracy of solutions obtained after a maneuver has been determined for a real measurement set. The preliminary results show that the accuracy of the kernel density method appears to be one order of magnitude better. However, this is only true as long as the maneuvers are predictable. The minimum energy solution can always serve as a fall-back option when no historic information is available. The analysis is only performed for a single satellite with a repeating pattern of maneuvers. Future studies will have to investigate the accuracy for more satellites and different maneuver types and strategies. Furthermore, future research should identify the extend of the historic data necessary to obtain accurate

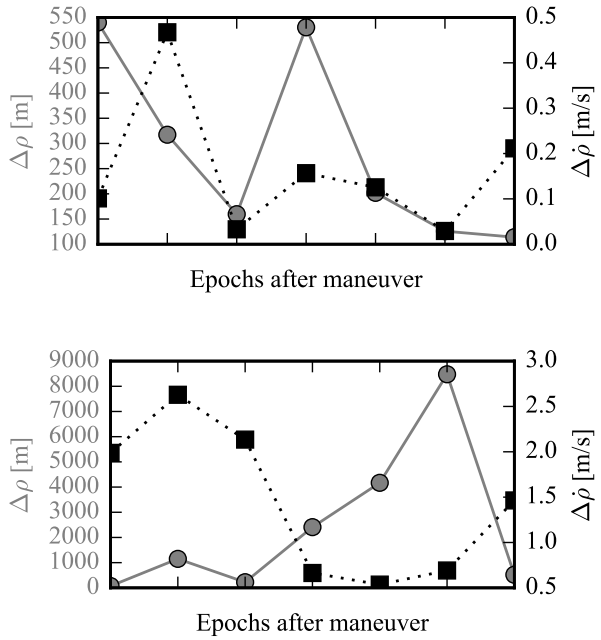

Figure 7: Difference between predicted and estimated post-maneuver states using the historic data (upper plot) and the minimum energy solution (lower plot) for 8 maneuver epochs of the Meteosat-9 dataset. The gray circles depict the range differences and the black squares depict the range-rate differences.

post-maneuver estimates, i.e. from which point on is the method capable to predict the future maneuvers. Additionally, the quality of the resulting orbits will be assessed further, e.g. if it suffices to successfully correlate the following observations with the determined state.

In the framework of space object behavior understanding, objects are classified into groups e.g. by the different operational maneuver strategies [1]. The catalog data (e.g. orbital states, measurements) can be merged with additional information sources (e.g. operator data, news articles, etc.) to describe the expected spacecrafts motion. If such a database is available, individual methods to predict the post-maneuver state depending on the satellite class could be developed. The here used kernel density estimation is a simple and robust way of describing the orbital change. However, more advanced prediction methods and more available object information can improve the performance. The principle idea of merging the new observations with the probable state density remains the same and could be also applied when using another density prediction tool.

REFERENCES

1. Furfaro, R. (2016). Resident Space Object Characterization and Behavior Understanding via Machine Learning and Ontology-based Bayesian Networks. *Advanced Maui Optical and Space Surveillance Technologies Conference*. (Maui, Hawaii, USA).
2. Holzinger, M. J., Scheeres, D. J., and Alfriend, K. T. (2012). Object correlation, maneuver detection, and characterization using control distance metrics. *Journal of Guidance, Control, and Dynamics* **35** (4), 1312–1325.
3. Houska, B., Ferreau, H. J., and Diehl, M. (2011). ACADO toolkit: An open-source framework for automatic control and dynamic optimization. *Optimal Control Applications and Methods* **32** (3), 298–312.
4. Kamel, A. A. (1982). Geosynchronous satellite perturbations due to Earth's triaxiality and luni-solar effects. *Journal of Guidance, Control, and Dynamics* **5** (2), 189–193.
5. Lemmens, S. and Krag, H. (2014). Two-line-elements-based maneuver detection methods for satellites in low earth orbit. *Journal of Guidance, Control, and Dynamics* **37** (3), 860–868.
6. Shabarekh, C. (2016). A Novel Method for Satellite Maneuver Prediction. *Advanced Maui Optical and Space Surveillance Technologies Conference*. (Maui, Hawaii, USA).
7. Singh, N., Horwood, J. T., and Poore, A. B. (2012). Space object maneuver detection via a joint optimal control and multiple hypothesis tracking approach. *Proceedings of the 22nd AAS/AIAA Space Flight Mechanics Meeting*. (Charleston, South Carolina, USA).
8. Jones, E., Oliphant, T., Peterson, P. *SciPy: Open source scientific tools for Python*. [Online; accessed 2016-12-01]. URL: `http://www.scipy.org/`.
9. Klinc, M. (2016). personal communication.
10. Milani, A. (2004). Orbit determination with very short arcs. I admissible regions. *Celestial Mechanics and Dynamical Astronomy* **90** (1-2), 57–85.
11. Parzen, E. (1962). On Estimation of a Probability Density Function and Mode. *The Annals of Mathematical Statistics* **33** (3), 1065–1076.
12. Silverman, B. W. (1986). *Density estimation for statistics and data analysis*. Vol. 26. CRC press.
13. Siminski, J., Fiedler, H., and Flohrer, T. (2017). Correlation of observations and orbit recovery considering maneuvers. *Proceedings of the 27th AAS/AIAA Space Flight Mechanics Meeting*. (San Antonio, Texas, USA).
14. Soop, E. M. (1994). *Handbook of geostationary orbits*. Vol. 3. Springer Science & Business Media.
15. Tommei, G., Milani, A., and Rossi, A. (2007). Orbit determination of space debris: admissible regions. *Celestial Mechanics and Dynamical Astronomy* **97** (4), 289–304.